Khakim2012_JPSE

by Artikel 6 Artikel 6

Submission date: 05-Apr-2023 06:58AM (UTC+0700)
Submission ID: 2056081293
File name: khakim2012_JPSE.pdf (3.44M)
Word count: 5762
Character count: 29851

Journal of Petroleum Science and Engineering 96-97 (2012) 152–161

Contents lists available at SciVerse ScienceDirect

Journal of Petroleum Science and Engineering

journal homepage: www.elsevier.com/locate/petrol

Geomechanical modeling for InSAR-derived surface deformation at steam-injection oil sand fields

M. Yusup Nur Khakim [a,b,*], Takeshi Tsuji [c], Toshifumi Matsuoka [a]

[a] Graduate School of Engineering, Kyoto University, C1-1-118 Kyotodaigaku-Katsura, Nishikyo-ku, Kyoto 615-8540, Japan
[b] Department of Physics, Sriwijaya University, Indonesia
[c] International Institute for Carbon-Neutral Energy Research, Kyushu University, Japan

ARTICLE INFO

Article history:
Received 20 January 2012
Accepted 6 August 2012
Available online 18 August 2012

Keywords:
steam injection
InSAR
inversion
modeling
monitoring

ABSTRACT

To estimate the distribution of reservoir deformation and reservoir volume change in an oil sand reservoir undergoing steam injection, we applied geomechanical inversion to surface uplift data derived from a differential interferometric synthetic-aperture radar (InSAR) stacking technique. We tested a two-step inversion method based on a tensional rectangular dislocation model. The first step of the inversion used genetic algorithms to estimate the depth of the reservoir and roughly model its deformation. The estimated depth of the reservoir was consistent with the depth of the injection point. The second step used a least-squares inversion with a penalty function and smoothing factor to efficiently invert the distribution of reservoir deformation and volume change from the surface uplift data. The distribution of reservoir deformation can be accurately estimated from InSAR-derived ground surface deformations using our proposed inversion techniques.

1. Introduction

Underground geomechanical instabilities due to rock and fluid manipulations, such as groundwater withdrawal, geothermal exploration, steam injection, and waste-water injection, can induce deformation in reservoirs. This reservoir deformation is largely induced by the change of reservoir pressure and consequently generates measurable surface deformations as subsidence or uplift. Excessive surface deformation can result in significant economic losses because of the failure of structures such as well casings, pipelines, and other underground utilities (Hu et al., 2004).

Teatini et al. (2011) presented the fundamental geomechanical processes that govern land uplift due to subsurface fluid injection for purposes such as enhanced oil recovery, storage of natural gas in depleted petroleum fields, recharge of overdrafted aquifer systems, and mitigation of anthropogenic land subsidence. The degree of uplift depends on a number of factors that include the pore fluid pressure increase and the depth, thickness and areal extent of the pressurized and heated geological formation.

GPS is well suited for surface deformation monitoring because it not only has high accuracy, but it also provides three components of surface deformation (Dixon et al., 1997). However, GPS surveys over large areas are labor intensive and time consuming. Another geodetic method, interferometric synthetic aperture radar (InSAR) technology, is capable of imaging small ground surface deformations (1 cm or less) over large areas in all weather conditions (Burgmann et al., 2000). Klees and Massonnet (1999) discussed potential applications of InSAR for monitoring deformations related to earthquake and crustal studies, monitoring volcanoes and anthropogenic effects, and monitoring glaciers and ice sheets. InSAR has been used to monitor surface deformation due to fluid injection at the Belridge and Lost Hills oil fields in California (e.g., Patzek and Silin, 2000; Patzek et al., 2001) and the CO_2 sequestration project at Krechba, Algeria (Mathieson et al., 2009; Du et al., 2010). More recent applications of this technology by the petroleum industry, which invert surface deformation measurements (using tiltmeters or InSAR) for reservoir level information, have been presented by Du et al. (2008), Maxwell et al. (2009) and Atefi Monfared and Rothenburg (2011).

Because surface uplift is induced by reservoir expansion, it is valuable information for estimating dynamic changes in reservoir properties. Characterization of surface deformation sources based on InSAR measurements has therefore become important in reservoir monitoring for activities such as enhanced oil recovery and CO_2 capture and storage projects. The amplitude and the rate of surface deformation are key parameters in optimizing economic production and minimizing environmental impact. A common application of these measurements is to numerically or analytically simulate the source of deformation.

* Corresponding author at: Kyoto University, Graduate School of Engineering, C1-1-118 Kyotodaigaku-Katsura, Nishikyo-ku, Kyoto 615-8540, Japan. Tel.: +81 75 383 3206; fax: +81 75 383 3203.
E-mail address: myusup_nkh@earth.kumst.kyoto-u.ac.jp (M.Y.N. Khakim).

0920-4105/$ - see front matter © 2012 Elsevier B.V. All rights reserved.
http://dx.doi.org/10.1016/j.petrol.2012.08.003

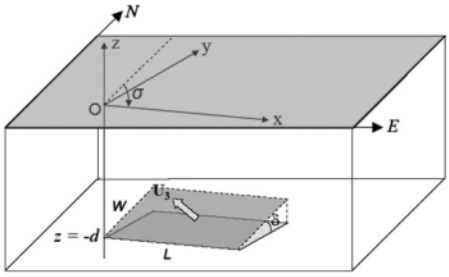

Fig. 1. Finite rectangular plane dislocation model.

Table 1
Notation of Okada's formulas.

Symbol	Quantity
u_z	Vertical displacement at surface
U_3	Vertical deformation in reservoir
y, d	Coordinates of the fault plane
ξ, η, q	Coordinates of the first point of the fault plane
R	Distance between first point of the fault plane and the origin
X	Coordinate of the point on the fault direction
L	Length of fault patch along strike
W	Width of fault patch along dip

Table 2
Inversion parameters.

I.	**Synthetic model parameters**		
1.	Length	2200 m	
2.	Width	1600 m	
3.	Depth of deformation source	500 m	
4.	Vertical reservoir deformation (average value of Fig. 2a)	2.09 cm	
5.	(x, y)-position	(3300, 2700) m	
6.	Strike	270°	
II.	**Inversion results**		**Relative error (%)**
1.	Length	1667 m	24.2
2.	Width	1700 m	6.3
3.	Depth of deformation source	499 m	0.2
4.	Vertical reservoir deformation	2.58 cm	23.4
5.	(x, y)-position	(2887 m, 2887 m)	(12.5, 6.9)
6.	Strike	279°	3.3
III.	**Initial model**		
1.	Length	500–3000 m	
2.	Width	500–2400 m	
3.	Depth of deformation source	100–600 m	
4.	Vertical reservoir deformation	0–4.00 m	
5.	(x, y)-position	(0–4000, 0–4000)m	
6.	Strike	0–360°	
7.	Crossover probability	0.7	
8.	Mutation probability	0.4	
9.	Number of generations	500	
10.	Number of individuals	800	

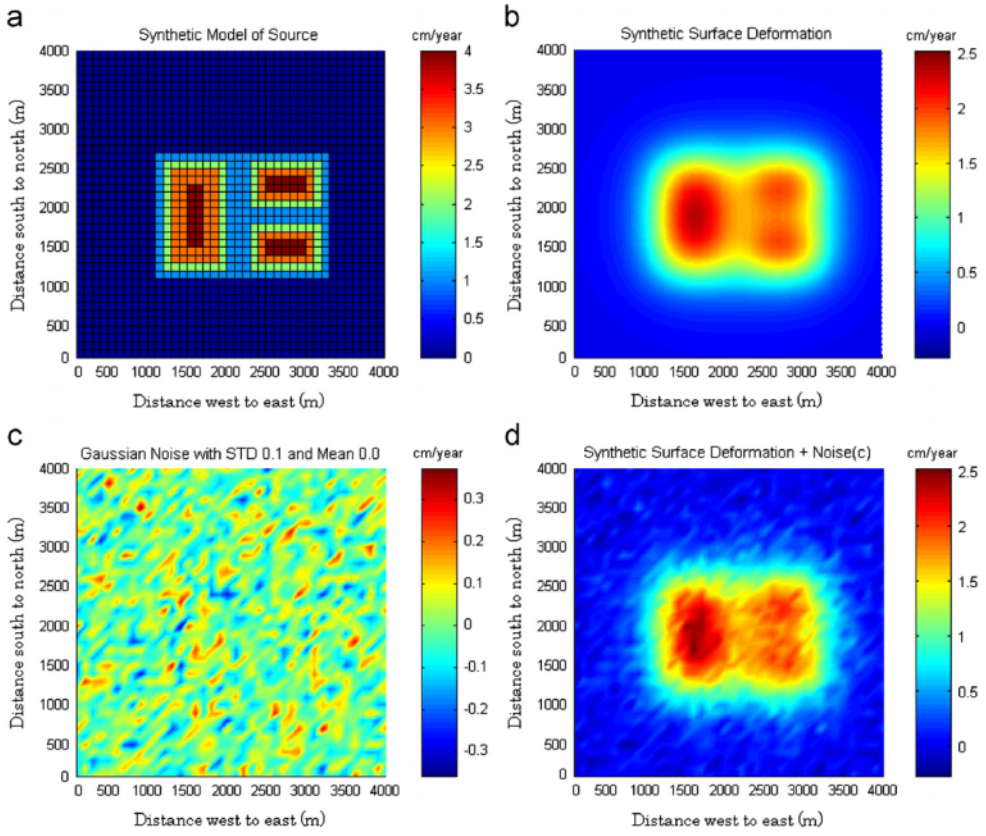

Fig. 2. (a) Synthetic model of reservoir deformation, (b) synthetic surface uplift resulting from forward modeling of reservoir deformation, (c) added noise, and (d) synthetic surface uplift with added noise.

Source models capable of simulating surface deformation include the point source (Mogi, 1958), ellipsoidal source (Yang et al., 1988), and rectangular source models (Okada, 1985). The first two are commonly used for volcano and reservoir modeling (Delaney and McTigue, 1994; Fialko and Simons, 2000; Oppliger et al., 2005). The third is mostly used for volcanic and seismic events (Jonsson et al., 2002; Anderssohn et al., 2009). A purely volumetric dilation source gives rise to a monopolar distribution of vertical displacement, whereas a shear distortion gives rise to a dipolar displacement field (Dusseault and Collins, 2008).

In this paper, we describe a two-step inversion scheme, starting from the surface uplift map obtained by InSAR measurement, to estimate the distribution of reservoir deformation and volume change rates where an oil sand reservoir is undergoing steam injection, or steam assisted gravity drainage (SAGD). In the first step, the geometry of reservoir deformation is estimated by inverting the uplift map adopting the source model of Okada (1985) using genetic algorithm (GA) inversion. In the second step, the least-squares method is used to obtain reservoir deformation, from which changes in reservoir volume can then be estimated.

2. Two-step inversion scheme

Ground surface uplift information derived from InSAR data provides an excellent opportunity to analyze physical processes of steam chamber development in an oil sand reservoir during the SAGD process. SAGD involves the use of high-pressure steam to liquefy bitumen for extraction. Two horizontal wells (or pipelines) are usually placed along the bottom of an oil sand formation, one above the other. Steam injected into the formation through the upper well heats the bitumen, which flows by gravity to the lower well where it is collected and pumped to the surface. The high pressure associated with SAGD deforms the reservoir and its surrounding lithology. This can be modeled as a deformation source pushing the overburden upward.

The uplift at a point on the ground surface induced by an arbitrary distribution of reservoir deformation can be expressed by the Volterra formula as

$$u_k(x) = \iint_{\sum} U_i(x') G_{ij}^k(x,x') n_j(x') d\sum(x') \tag{1}$$

where $u_k(x)$ is the ground surface displacement at x, $U_i(x')$ is the reservoir deformation at x', n_j is the normal to the surface Σ, and G_{ij}^k is the Green's function relating unit reservoir deformation in the i direction at x' to the ground surface displacement in the k direction at x (Du et al., 1992).

Eq. (1) shows that the surface displacement is the product of the Green's function G_{ij}^k and reservoir deformation $U_i(x')$. Therefore the inverse problem with respect to observed displacements $u_k(x)$, without any constraints, is a nonlinear problem. In this paper, we approach the nonlinear inverse problem by starting from surface uplift as measured by InSAR data, but there is no prior information related to the reservoir itself, which may happen when the distribution of injected steam is not precisely known.

To approach this nonlinear problem, we adopted a two-step inversion scheme using a GA inversion to identify the geometry of the steamed zone (first step) and then using a least-squares inversion to estimate the reservoir volume change (second step). In both steps we adopt the Green's function for an elastic, homogeneous, and isotropic half-space with tensile dislocation plane movements, known as Okada's formula (Okada, 1985), to evaluate surface displacements. This model is simple and is suitable for inversion.

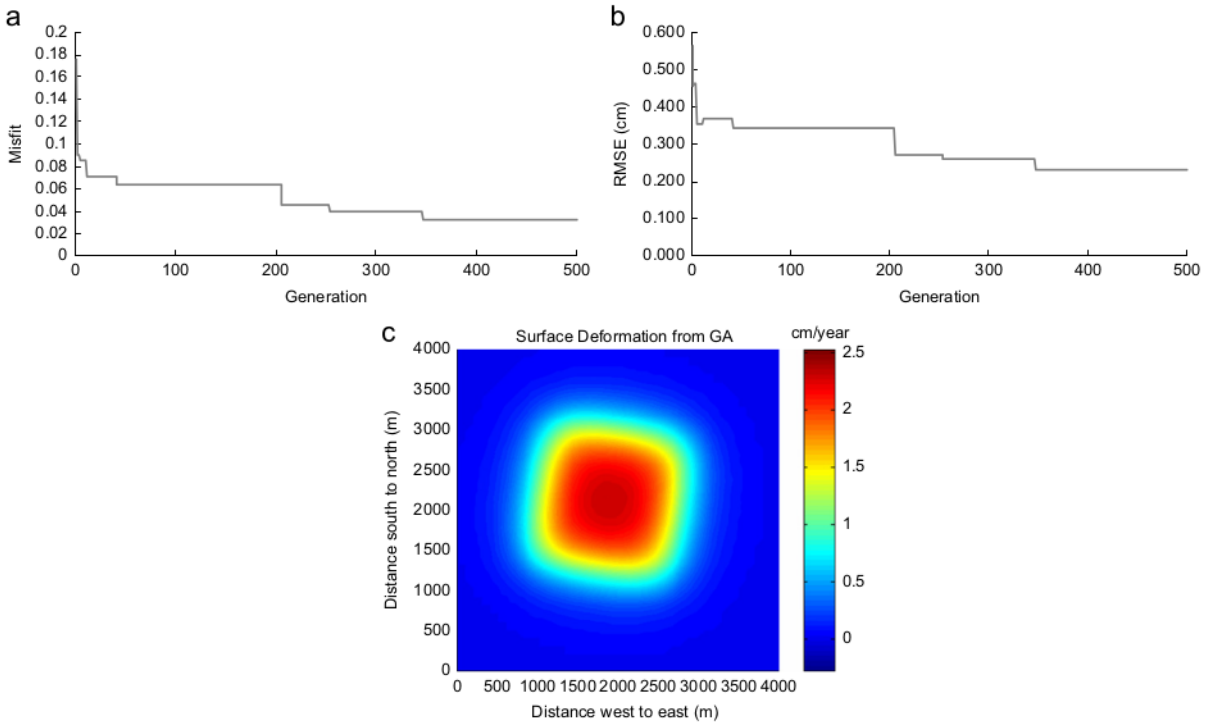

Fig. 3. (a) Misfit, (b) RMSE, and (c) surface uplift resulting from the solution of the GA inversion.

Okada (1985) provided analytical expressions to describe the surface deformation due to dislocation of a fault patch by strike–slip, dip–slip, and tensile fault movements. The component of vertical displacement (u_z) for the rectangular-tensional dislocation model (Fig. 1) can be expressed as (Okada, 1985, 1992):

$$u_z = \frac{U_3}{2\pi}\left[\frac{\tilde{y}q}{R(R+\xi)} + \cos\delta\left\{\frac{\xi q}{R(R+\eta)}\tan^{-1}\frac{\xi\eta}{qR}\right\} - I_5\sin^2\delta\right]\Big\|, \tag{2}$$

where

$$I_5 = \frac{\mu}{\lambda+\mu}\frac{2}{\cos\delta}\tan^{-1}\frac{\eta(X+q\cos\delta)+X(R+X)\sin\delta}{\xi(R+X)\cos\delta} \tag{3}$$

and

$$\begin{aligned} p &= y\cos\delta + d\sin\delta;\\ q &= y\sin\delta - d\cos\delta;\\ \tilde{y} &= \eta\cos\delta + q\sin\delta;\\ \tilde{d} &= \eta\sin\delta - q\cos\delta\\ R^2 &= \xi^2+\eta^2+q^2 = \xi^2+\tilde{y}^2+\tilde{d}^2\\ X^2 &= \xi^2+q^2 \end{aligned} \tag{4}$$

and Chinnery's notation $\|$ represents the substitution:

$$f(\xi,\eta)\| = f(x,p) - f(x,p-W) - f(x-L,p) + f(x-L,p-W). \tag{5}$$

Notations for these four expressions are listed in Table 1.

The coordinates of the origin of the fault patch (lower left-hand corner) are E, N, and d, taken as positive in the east, north, and down directions, respectively. The strike of the fault (σ) is expressed in degrees clockwise from north to transform the (x, y) coordinate system of Okada (1985). Eq. (2) corresponds to Eq. (1) for the case of simple rectangular plane deformation. Also in Eq. (2), the surface deformation u_z is proportional to the amount of subsurface deformation U_3 and the dislocation depth d (Fig. 1). Therefore, we need to solve a nonlinear inversion problem with respect to U_3 and the depth of dislocation.

From Eqs. (2) to (5), the surface displacement depends on the medium constants, λ and μ. However, underground deformation that is parallel to the surface of a semi-infinite elastic body corresponds to $\delta=0$, so that the last term on the right-hand side of Eq. (2), which contains λ and μ (Eq. (3)), becomes zero (Okada, 1985). This special case of u_z is independent of medium constants.

2.1. GA inversion for geometry of deformation source (first step)

We adopted a global optimization approach based on the use of GAs (Goldberg, 1989) to deal with nonlinear inversion problems. The first step of our inversion scheme is to estimate reservoir deformation parameters such as geometry (width and length), horizontal (x, y) position, depth, orientation (strike), and uniform magnitude of rectangular vertical deformation, from the ground surface uplift obtained by InSAR.

GAs are based on the analogy of using biological evolution to find the fittest individual by defining an objective function (Goldberg, 1989). A randomly generated initial population of starting models is subjected to change by systematically approaching the best solution among many investigated solutions. The model parameters are represented by binary digits or bit strings. The major GA operators of evaluation, reproduction, crossover and mutation modify the population in the search for the best solution of the reservoir deformation parameters.

The searching process is terminated after enough iterations to achieve a stopping criterion, that is, to minimize a misfit function. The lower the misfit function, the closer an individual in the population is to the optimal solution. In this paper, we adopted the following misfit function, which is more appropriate for larger N (Nunnari et al., 2005):

$$J = \frac{\sum_{i=1}^{N}(P_i-O_i)^2}{\sum_{i=1}^{N}(|P_i-\overline{O}|+|O_i-\overline{O}|)^2}. \tag{6}$$

In Eq. (6), N is the number of data points on the surface, and O_i and P_i are the observed and calculated values of surface deformation, respectively. To evaluate the error related to this inverse modeling approach, we calculated the root mean square error (RMSE) using

$$RMSE = \sqrt{\frac{1}{N}\sum_{i=1}^{N}(P_i-O_i)^2}. \tag{7}$$

2.2. Least-squares inversion for reservoir volume change (second step)

The GA inversion estimates the reservoir deformation parameters as described in Section 2.1; however, the simple Okada model provides a single dislocation with uniform vertical deformation and is not suitable for direct use with real data. A uniform deformation inadequately represents the spatially varying vertical deformation in an oil sand reservoir. To overcome this problem, the rectangle is divided into a grid in which each grid point can have a different deformation.

Using this gridded model, Eq. (1) can be recast as a set of linear equations for InSAR data at many observation points as follows

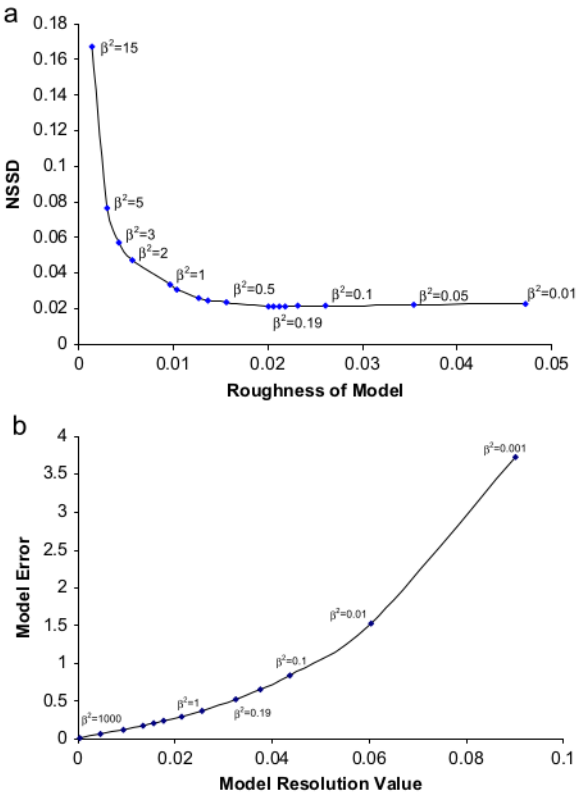

Fig. 4. Trade-off curves for synthetic data between (a) roughness and NSSD of solution and (b) model error and model resolution.

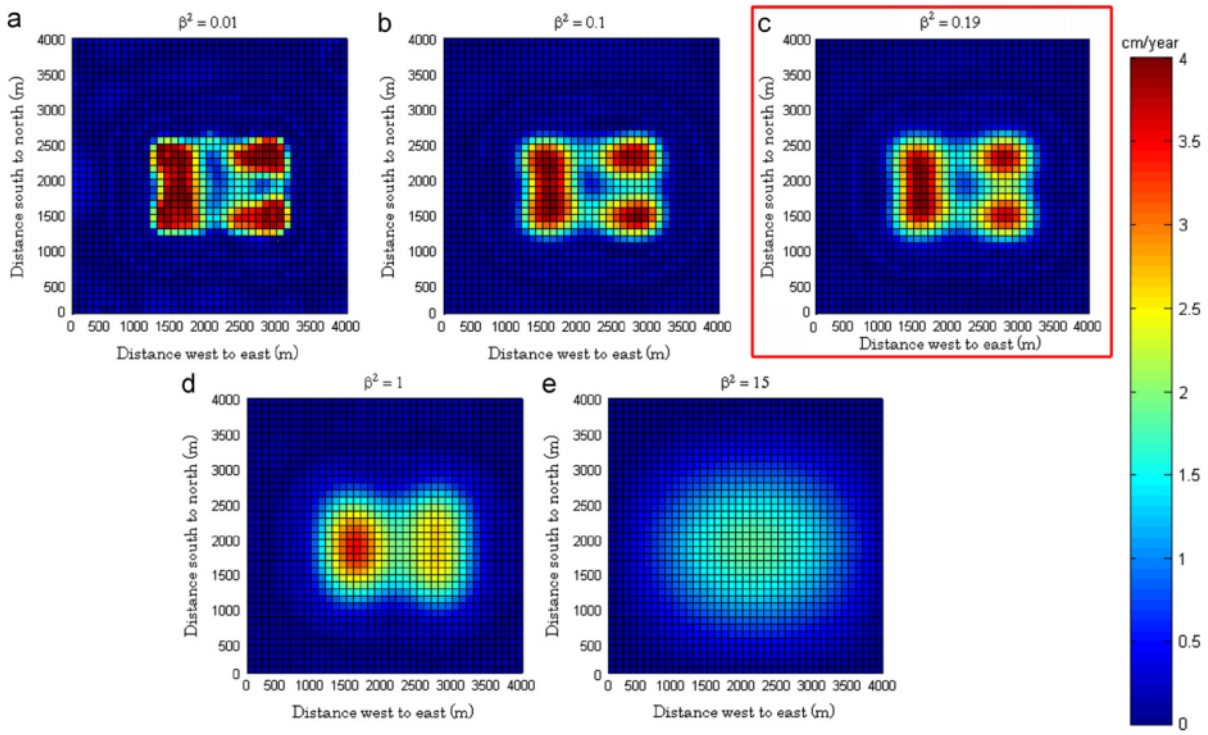

Fig. 5. Modeled reservoir deformations resulting from the solution of least-squares inversion using a smoothing factor (β^2) of (a) 0.01, (b) 0.1, (c) 0.19, (d) 1.0, and (e) 15.

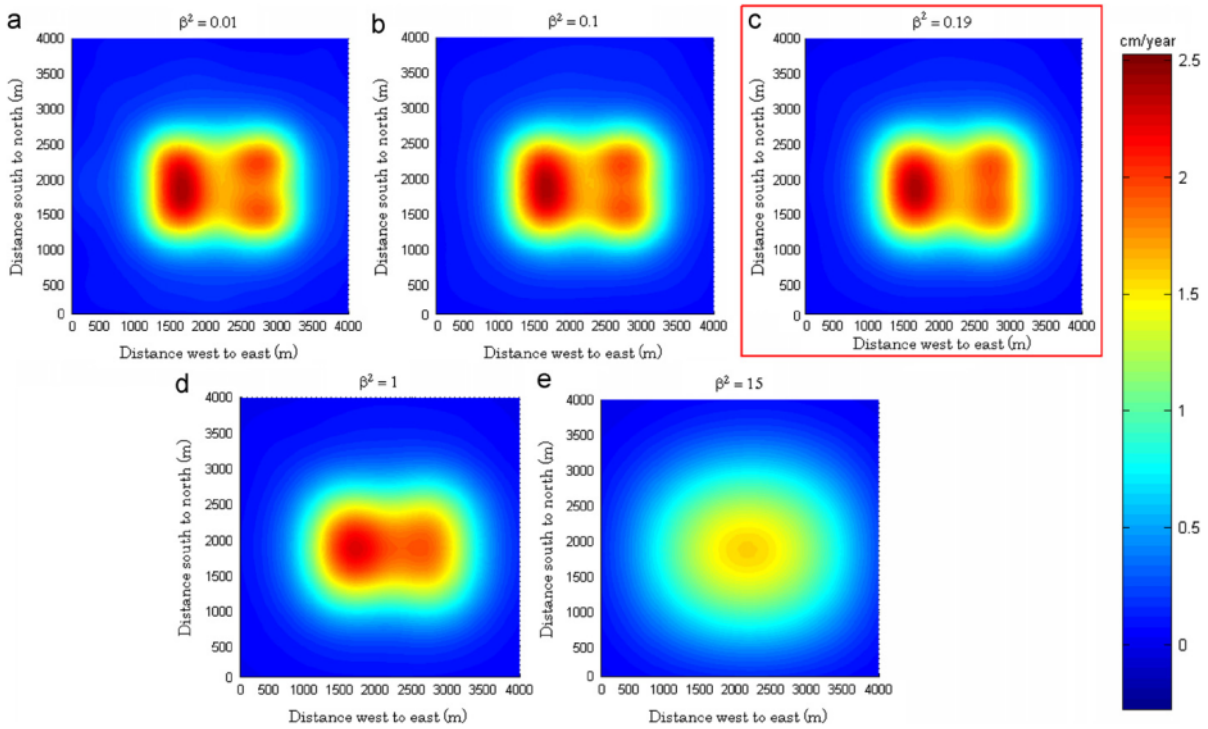

Fig. 6. Surface uplift maps resulting from the solution of least-squares inversion using a smoothing factor (β^2) of (a) 0.01, (b) 0.1, (c) 0.19, (d) 1.0, and (e) 15.

(Du et al., 1992):

$$\mathbf{d} = \mathbf{Gm}, \tag{8}$$

where $\mathbf{d}$ is the vector of n surface uplift values, $\mathbf{G}$ is a known $n \times m$ matrix for a given depth and grid size, and $\mathbf{m}$ is the vector of m unknown reservoir deformations, which are vertical deformations. This discrete approximation can sufficiently approximate the true continuous reservoir deformations (i.e., integral Eq. (1)) when grid size is reasonably small.

In many cases, the inverse problem becomes ill-posed, and the solution is not unique (Menke, 1984). In such cases, the inverse problem can be regularized by adding information. This information is translated into a penalty function that is added to the objective function, which is then minimized to estimate the distribution of reservoir deformations:

$$F = \|\mathbf{Gm}-\mathbf{d}\|^2 + \beta^2 \|\mathbf{Hm}-\mathbf{d_0}\|^2, \tag{9}$$

where the first term is the norm of the residuals between calculated and observed data, β^2 is a penalty (smoothness) factor that weights the prior information $\mathbf{Hm}=\mathbf{d_0}$ ($\mathbf{d_0}$ are equal to zero), and $\mathbf{H}$ is the discrete Laplacian operator.

The penalty factor β^2 plays the role of trade-off parameter between the fitness and roughness of the model. The model roughness is defined by $\|\mathbf{Hm}\|^2$, which increases with decreasing β^2. The sum of the normalized squared differences (NSSD) is introduced as a function of the model roughness for the variation of β^2 that yields a reasonable model of reservoir deformation. The best solution for the inversion problem has also to be chosen from the trade-off curve between model error and model resolution (Du et al., 2010). The best solution is the one that combines acceptable error and reasonable resolution.

Once the distribution of reservoir deformations is estimated, a map of volume change at each grid point can be obtained by multiplying the grid size and vertical reservoir deformation in each grid cell. From this map, the total volume change can be calculated by summation of the individual volume changes. This calculation assigns only volume changes in the vertical direction to the reservoir grid cells.

3. Results and discussion

3.1. Application to synthetic model

To examine the performance of our two-step inversion scheme, we prepared a synthetic model of reservoir deformation with magnitudes ranging from 1 to 4 cm (Fig. 2a). The deformation source is located at a depth of 500 m. There are three uplift maxima in the west, northeast, and southeast parts of the reservoir. The volume change due to the deformation in this model is 7.36×10^4 m^3. The synthetic model is 2200 m long from east to west and 1600 m wide from north to south with a strike of N90°E. From this synthetic model, we applied forward modeling based on Okada's formula to obtain a synthetic uplift map (Fig. 2b) and then added Gaussian noise (Fig. 2c) with a mean of 0.0 and standard deviation of 0.1 cm to the map to generate noisy synthetic uplift (Fig. 2d) as an inversion input.

Using random initial models (Table 2), we initially applied GA inversion to the synthetic uplift map (Fig. 2d). We evaluated individual solutions by the misfit between the observed and calculated surface uplift. Minimizing the misfit means maximizing the performance to find the best solution. After 500 generations

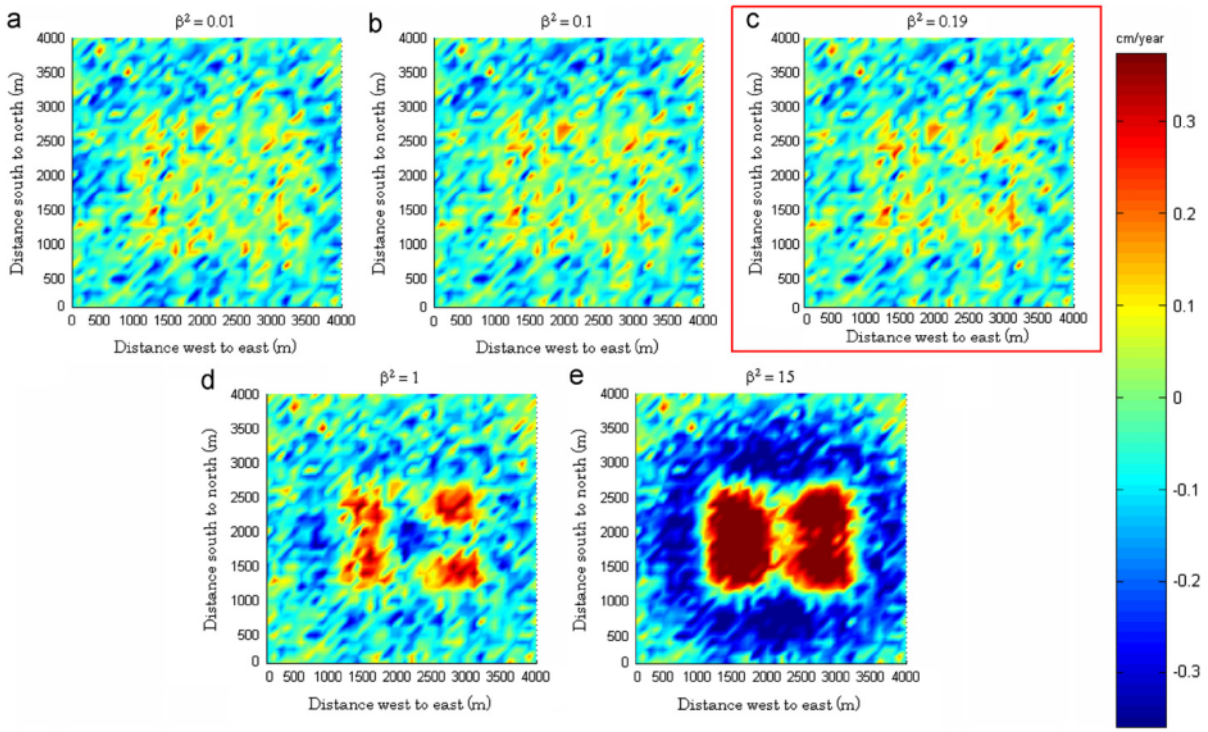

Fig. 7. Residual between the noisy synthetic uplift and the calculated uplift from the solution of least-squares inversion using a smoothing factor (β^2) of (a) 0.01, (b) 0.1, (c) 0.19, (d) 1.0, and (e) 15.

(Fig. 3a), the misfit of the solution declined to 0.0324 and the RMSEs of the solution (Fig. 3b) declined to 0.23 cm, which reflects the presence of the added noise.

The GA inversion results (Table 2) show that the depth of the deformation source, which is the most important parameter controlling surface deformation, can be estimated within a relative error of 0.2% for source depths between 100 m and 600 m. Because the variation in the vertical deformation over the reservoir makes comparisons difficult, we compared the average value of the synthetic model deformation to the deformation obtained from the global GA solution and found relative errors as great as 23.4%. However, the shape of the surface uplift obtained from the GA inversion (Fig. 3c) is quite different from that in the synthetic model (Fig. 2b), having a single uplift maximum in the inversion solution versus three in the synthetic data. Therefore, the reservoir deformation from the GA inversion is considered to be a rough estimate.

To improve reservoir deformation solutions for heterogeneous fields, we applied a least-squares technique as the second step of our inversion. In this step, we divided the ground surface and reservoir of the synthetic model into a 40×40 grid to yield 1600 square elements with sides of 100 m. We used a penalty function with smoothing factors (β^2) in this least-squares inversion to search for the optimum distribution of reservoir deformation. Although larger smoothing factors yielded smoother vertical reservoir deformations, the NSSDs became larger. Therefore, we investigated the trade-off curve between the roughness of the deformation distribution and the NSSD as the smoothing factor varied (Fig. 4a) and the trade-off curve between the model error and the model resolution value (Fig. 4b) (Du et al., 2010). We chose a smoothing factor of 0.19 to obtain the best solution of the distribution of reservoir deformations (Fig. 5c).

More detailed results of the least-squares inversion are shown in Fig. 5. Smoothing factors (β^2) less than 0.19 resulted in solutions clearly showing three separate areas of deformation (Fig. 5a and b), similar but not identical to those in the synthetic model (Fig. 2a). With smoothing factors larger than 0.19, the inversion could not resolve three deformation areas (Fig. 5d and e).

To evaluate the performance of this inversion, we used the inversion results to synthesize a map of surface uplift (Fig. 6c)

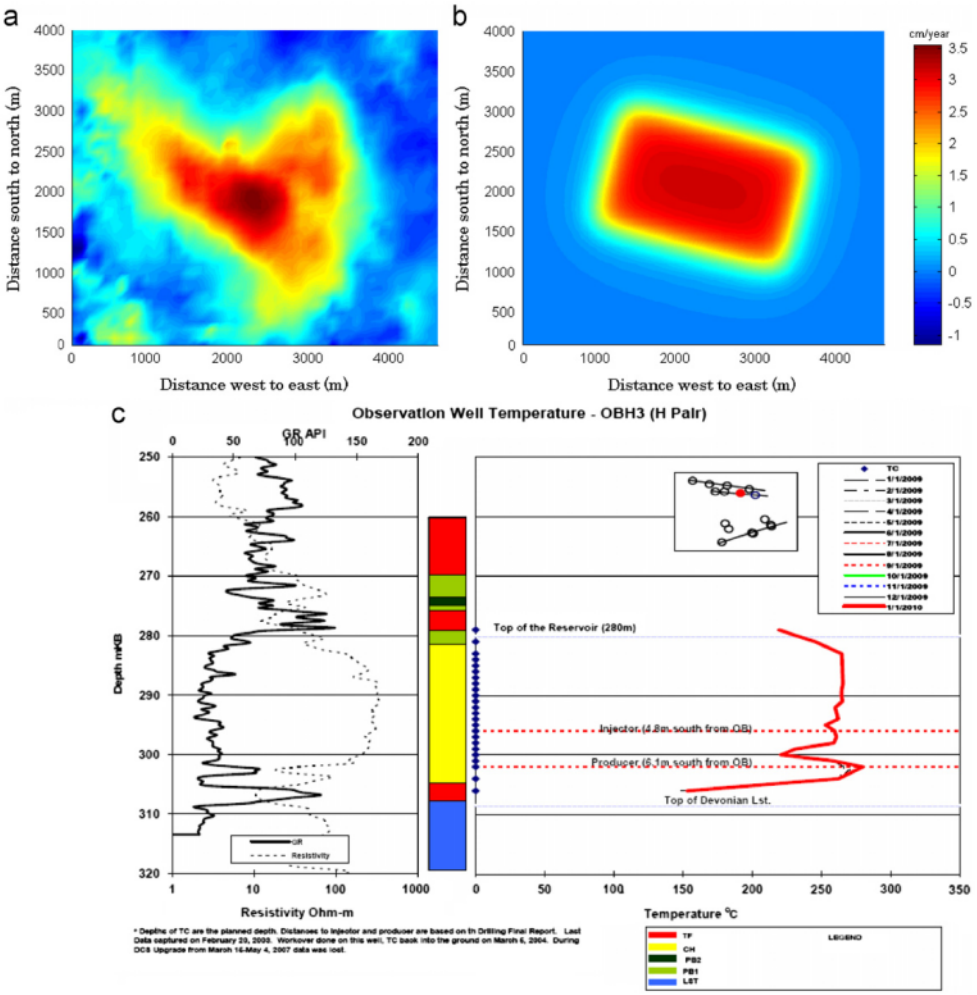

Fig. 8. (a) Observed surface vertical displacement from InSAR data, (b) modeled vertical surface displacement from the GA method, and (c) borehole data showing the depth of injection (JACOS, 2009).

that closely resembled the synthetic model map (Fig. 2b). The residuals between the synthetic model and the calculated surface uplift (Fig. 7c) were comparable to the input of noise in the synthetic model (Fig. 2c). The RMSE with the optimum smoothing factor (Fig. 4b) was 0.114 cm whereas the standard deviation of the additive noise was 0.100 cm, and the residual map in Fig. 7c was also close to the input error in our synthetic model. Because these errors were comparable, we considered our simulation approach acceptable and consequently applied it to real data from an oil sand field.

3.2. Application to real deformation data

In this study we made use of seven images acquired by the Phase Array type L-band SAR (PALSAR) instrument on the Japanese Advanced Land Observation Satellite (ALOS) "Daichi" for the period from 9 February 2007 to 30 December 2008. The data were the high-bandwidth (FBS, 28 MHz) and low-bandwidth (FBD, 14 MHz) modes from ascending orbits with an off-nadir angle of 34.3°. The data processing steps included SAR processing, interferometric processing, geocoding, topographic phase removal, adaptive filtering, and phase unwrapping (Simons and Rosen, 2007). To reduce some noise sources, such as atmospheric effects, we performed quadratic-phase removal and stacking of unwrapped phases. Finally, we converted the stacked unwrapped phase to vertical displacement rates for this application of the proposed method.

The InSAR deformation map estimated by the stacking technique from six interferograms was inverted using our two-step method. Fig. 8 compares the observed vertical surface displacement map (Fig. 8a) and the modeled vertical surface displacement map as estimated by the GA inversion in the first step (Fig. 8b). We constrained the lower and upper bounds of length, width, depth, chamber development (vertical displacement) and strike of the dislocation plane (considered as the steam chamber in this case) to 800–3000 m, 800–3000 m, 200–300 m, 0–1 m and 0°–360°, respectively, in our search space. We also adopted a dip angle of zero as one of the inversion parameters and used the initial population of 800 individuals and 500 generations of modeling. To maintain diversity in the population and sustain the convergence capacity of the GA, we defined values of 0.7 and 0.4 for the probabilities of crossover and mutation, respectively.

The GA inversion yielded a best-fit model predicting a rectangular dislocation plane with length, width and depth of 2413 m, 1533 m and 297 m, respectively, with a RMSE of 0.627 cm. The depth of the deformation source was in good agreement with the depth of the steam injection wells (Fig. 8c).

To estimate the detailed deformation of the reservoir from the surface uplift estimated from InSAR data, we used a penalty function in the least-squares inversion (Du et al., 1992) as we did with the synthetic model. The best-fit single dislocation plane model from the GA inversion was enlarged to a $4.6 \times 4.0\ km^2$ horizontal dislocation plane that was then discretized into $100 \times 100\ m^2$ patches for inversion of distributed-source deformation. We tested five smoothing factors (0.001, 0.01, 0.1, 1, and 10), and analyzed the trade-off curves between roughness and NSSD (Fig. 9a) and between model error and model resolution value (Fig. 9b) (Du et al., 2010). For the lowest smoothing factor ($\beta^2 = 0.001$) the reservoir vertical deformation rate was highly oscillatory (Fig. 10a), and for the highest smoothing factor ($\beta^2 = 10$), the reservoir vertical deformation was overly smooth (Fig. 10e). A smoothing factor of 0.1 yielded a reservoir deformation pattern (Fig. 10c) that was closely related to well locations (Fig. 10f).

The map of modeled surface displacement (Fig. 11c) is comparable to the observed uplift (Fig. 11f) with a RMSE of 0.125. The

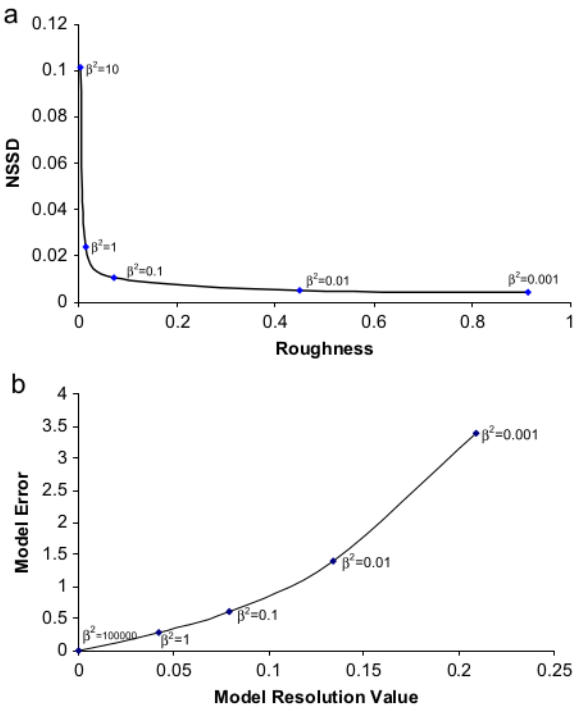

Fig. 9. Trade-off curves for real data between (a) roughness and NSSD of solution and (b) model error and model resolution.

small residuals between the observed and modeled displacements may be related to noise in the InSAR data, especially atmospheric artifacts. Using larger smoothing factors yielded smoother surface uplifts, as shown in Fig. 11d and e. Smaller smoothing factors yielded surface uplift maps that were more similar to the observed uplift, but the NNSD became larger.

By multiplication of the grid size and vertical reservoir deformation in each corresponding grid, we obtained a map of volume change at each grid point. Finally, using Okada's simple tensile dislocation model, we determined that the total volume change rate was 150,809 m^3/yr by summation of the individual volume changes. This volume change rate may be considered an estimate of steam chamber growth during the SAGD process.

4. Conclusion

To evaluate the deformation of an oil sand reservoir caused by steam injection, we proposed a two-step inversion approach using InSAR-derived surface deformation data. The first step is solving a nonlinear inversion using the GA method and estimating the depth of the deformation zone. The second step is solving a linear inversion using the least-squares method and estimating the distribution of the subsurface deformation in detail. This methodology can be applied to cases with unknown reservoir depth using InSAR data alone.

We applied the GA method to the field data and roughly estimate the reservoir deformation based on surface vertical uplifts. The resulting depth of the target reservoir was in good agreement with the depths of injection points in boreholes. We then applied the penalty function technique in the least-squares

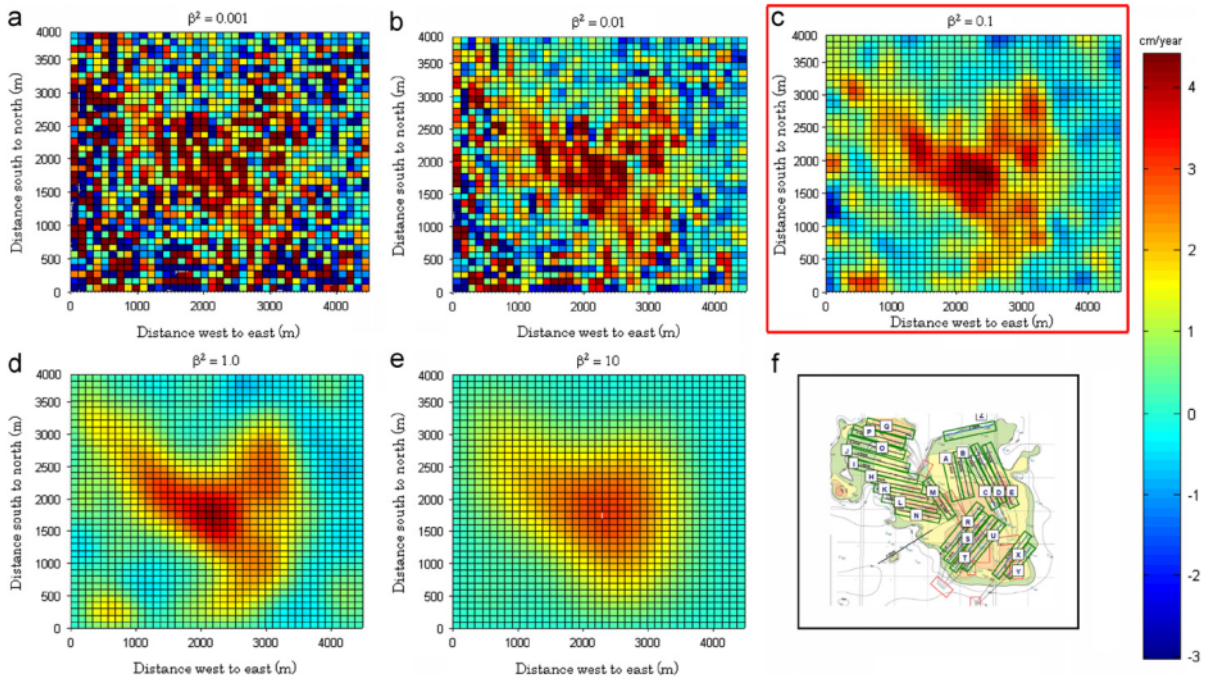

Fig. 10. Modeled reservoir deformations resulting from the solution of least-squares inversion using a smoothing factor (β^2) of (a) 0.001, (b) 0.01, (c) 0.1, (d) 1 and (e) 10, and (f) configuration of production and injection wells (JACOS, 2009).

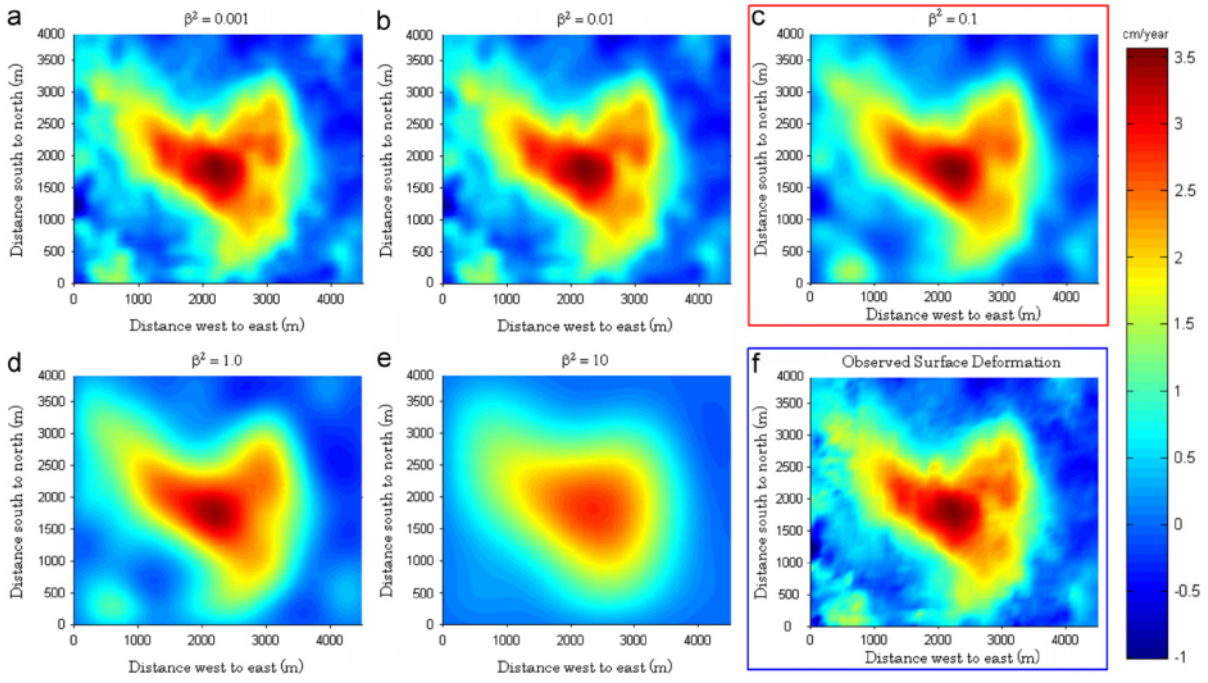

Fig. 11. Modeled surface vertical displacements using a smoothing factor (β^2) of (a) 0.001, (b) 0.01, (c) 0.1, (d) 1 and (e) 10, and (f) observed data from InSAR.

inversion with a smoothing factor to estimate the best vertical deformation rate. This technique yielded a vertical deformation distribution in good agreement with the configuration of wells in the oil sand field. Because surface deformation maps can be obtained on a frequent basis from InSAR analysis, we can monitor the growth of steam chambers using our approach.

Acknowledgments

We thank the Science and Technology Research Partnership for Sustainable Development (SATREPS), a collaboration between the Japan Science and Technology Agency (JST) and the Japan International Cooperation Agency (JICA), for financial support and the Earth Remote Sensing Data Analysis Center (ERSDAC) for providing ALOS PALSAR data. The Japan Ministry of Economy, Trade and Industry (METI) and the Japan Aerospace Exploration Agency (JAXA) are owners of the ALOS PALSAR original data. The PALSAR Level-1.0 products were produced by ERSDAC. The first author thanks the Indonesia Ministry of National Education for financial support during his study at Kyoto University and thanks K. Ishitsuka of Kyoto University for discussions of inversion. T. Tsuji gratefully acknowledges the support of the International Institute for Carbon Neutral Energy Research (WPI-I2CNER), sponsored by the World Premier International Research Center Initiative (WPI), MEXT, Japan.

References

Anderssohn, J., Motagh, M., Walter, T.R., Rosenau, M., Kaufmann, H., Oncken, O., 2009. Surface deformation time series and source modeling for a volcanic complex system based on satellite wide swath and image mode interferometry: the Lazufre system, central Andes. Remote Sens. Environ. 113, 2062–2075.

Atefi Monfared, K., Rothenburg, L., 2011. Reconstruction of reservoir deformations from ground surface tilt measurements: effects of monitoring strategies. In: Proceedings of the ARMA 11-174, presented at the 45th US Rock Mechanics/Geomechanics Symposium, San Francisco, CA, June 26–29.

Burgmann, R., Rosen, P.A., Fielding, E.J., 2000. Synthetic aperture radar interferometry to measure earth's surface topography and its deformation. Annu. Rev. Earth Planet. Sci. 28, 169–209.

Delaney, P.T., McTigue, D.F., 1994. Volume of magma accumulation or withdrawal estimated from surface uplift or subsidence, with application to the 1960 collapse of Kilauea Volcano. Bull. Volcanol. 56, 417–424.

Dixon, T.H., Mao, A., Bursik, M., Heflin, M., Langbein, J., Stein, R., Webb, F., 1997. Continuous monitoring of surface deformation at Long Valley Caldera, California, with GPS. J.Geophys. Res. 102, 12017–12034.

Du, Y., Aydin, A., Segall, P., 1992. Comparison of various inversion techniques as applied to the determination of a geophysical deformation model for the 1983 Borah Peak earthquake. Bull. Seismol. Soc. Am. 82, 1840–1866.

Du, J., Brissenden, S.J., McGillivray, P., Bourne, S., Hofstra, P., Davis, E.J., Roadarmel, W.H., 2008. Mapping reservoir volume changes during cyclic steam stimulation using tiltmeter-based surface deformation measurements. SPE Reservoir Eval. Eng. 11 (1), 63–72 (SPE-97848-PA, February).

Du, J., McColpin, G.R., Davis, E.J., Marsic, S., 2010. Model uncertainties and resolution studies with application to subsurface movement of a CO_2 injection project in the Krechba field using InSAR data. J. Can. Petrol. Technol. 49 (6) (SPE-138969-PA, June).

Dusseault, M.B., Collins, P.M., 2008. Geomechanics effects in thermal processes for heavy oil exploitation. CSEG Rec., 20–23, June.

Fialko, Y., Simons, M., 2000. Deformation and seismicity in the Coso geothermal area, Inyo County, California: observations and modeling using satellite radar interferometry. J. Geophys. Res. 105, 21781–21794.

Goldberg, D.E., 1989. Genetic Algorithms in Search Optimization and Machine Learning. Addison-Wesley Publ. Co..

Hu, R.L., Yue, Z.Q., Wang, L.C., Wang, S.J., 2004. Review on current status and challenging issues of land subsidence in china. Eng. Geol. 76, 65–77.

JACOS, 2009. Hangingstone Demonstration Project 2008: Thermal In-Situ Scheme Progress Report. Approval no. 8788 G, presented on March 23, 2009.

Jonsson, S., Zebker, H., Segall, P., Amelung, F., 2002. Fault slip distribution of the 1999 Mw 7.1 Hector Mine, California, earthquake, estimated from satellite radar and GPS measurements. Bull. Seismol. Soc. Am. 92 (4), 1377–1389.

Klees, R., Massonnet, D., 1999. Deformation measurements using SAR interferometry: potential and limitations. Geol. Minjbouw 77, 161–176.

Mathieson, A., Wright, I., Roberts, D., Ringrose, P., 2009. Satellite imaging to monitor CO_2 movement at Krechba, Algeria. Energy Proc. 1, 2201–2209.

Maxwell, S.C., Du, J., Shemeta, J., Zimmer, U., Boroumand, N., Griffin, L.G., 2009. Monitoring SAGD steam injection using microseismicity and tiltmeters. SPE Reserv. Eval. Eng., 311–317 (SPE 110634-PA, April).

Menke, W., 1984. Geophysical Data Analysis: Discrete Inverse Theory. Academic Press Inc..

Mogi, K., 1958. Relations between the eruptions of various volcanos and the deformations of the ground surfaces around them. Bull. Earthquake Res. Inst., Univ. Tokyo 36, 99–134.

Nunnari, G., Puglisi, G., Guglielmino, F., 2005. Inversion of SAR data in active volcano areas by optimization techniques. Nonlinear Process Geophys. 12, 863–870.

Okada, Y., 1985. Surface deformation due to shear and tensile faults in a half space. Bull.Seismol. Soc. Am. 75, 1135–1154.

Okada, Y., 1992. Internal deformation due to shear and tensile fault in a half-space. Bull.Seismol. Soc. Am. 82, 1018–1040.

Oppliger, G., Mark, C., Shevenell, L., Taranik, J., 2005. Elucidating deep reservoir geometry and lateral outflow through 3-D elastostatic modeling of satellite radar (InSAR) observed surface deformations: an example from the Bradys geothermal field. Trans.—Geotherm. Resour. Counc. 29, 419–424.

Patzek, T.W., Silin, D.B., 2000. Use of INSAR in Surveillance and Control of a Large Field Project. Lawrence Berkeley National Laboratory.

Patzek, T.W., Silin, D.B., Fielding, E., 2001. Use of satellite radar images in surveillance and control to two giant oilfields in California. In: Proceedings of the SPE Annual Technical Conference and Exhibition, New Orleans, 30 September–3 October.

Simons, M., Rosen, P.A., 2007. Interferometric synthetic aperture radar geodesy. Treatise Geophys: Geodesy, T.A. Herring, ed., Elsevier 3, 391–446.

Teatini, P., Gambolati, G., Ferronato, M., Settari, A., Walters, D., 2011. Land uplift due to subsurface fluid injection. J. Geodyn. 51, 1–16.

Yang, X.M., Davis, P.M., Dieterich, J.H., 1988. Deformation from inflation of a dipping finite prolate spheroid in an elastic half-space as a model for volcanic stressing. J. Geophys. Res. 93, 4249–4257.

Khakim2012_JPSE

ORIGINALITY REPORT

10%	%	10%	%
SIMILARITY INDEX	INTERNET SOURCES	PUBLICATIONS	STUDENT PAPERS

MATCH ALL SOURCES (ONLY SELECTED SOURCE PRINTED)

1%

★ Takatoshi Kiriyama, Yosuke Higo. "Axisymmetric particle-element coupled method for deformation problems of geomaterial", Soils and Foundations, 2022

Publication

Exclude quotes	Off	Exclude matches	Off
Exclude bibliography	On		